

Article

Adsorption of Omeprazole on Biobased Adsorbents Doped with Si/Mg: Kinetic, Equilibrium, and Thermodynamic Studies

Roberta A. Teixeira ¹ , Pascal S. Thue ² , Éder C. Lima ³ , Alejandro Grimm ⁴ , Mu. Naushad ⁵,
Guilherme L. Dotto ⁶  and Glaydson S. dos Reis ^{4,*} 

¹ Graduate Program in Water Resources and Environmental Sanitation, Hydraulic Research Institute (IPH), Federal University of Rio Grande do Sul (UFRGS), Porto Alegre 91501-970, RS, Brazil; roberta.arleu@gmail.com

² Environmental Science Graduate Program, Engineering Center, Federal University of 8 Pelotas (UFPel), 989 Benjamin Constant St., Pelotas 96010-020, RS, Brazil; pascalsilasthue@gmail.com

³ Institute of Chemistry, Federal University of Rio Grande do Sul–UFRGS, Av. Bento Gonçalves 9500, P.O. Box 15003, Porto Alegre 91501-970, RS, Brazil; profederlima@gmail.com

⁴ Department of Forest Biomaterials and Technology, Biomass Technology Centre, Swedish University of Agricultural Sciences, SE-901 83 Umeå, Sweden; alejandro.grimm@slu.se

⁵ Department of Chemistry, College of Science, King Saud University, P.O. Box 2455, Riyadh 11451, Saudi Arabia; shad123@gmail.com

⁶ Research Group on Adsorptive and Catalytic Process Engineering (ENGEPA), Federal University of Santa Maria, Av. Roraima, 1000-7, Santa Maria 97105-900, RS, Brazil; guilherme_dotto@yahoo.com.br

* Correspondence: glaydson.simoedosreis@slu.se

Abstract: This paper proposes an easy and sustainable method to prepare high-sorption capacity biobased adsorbents from wood waste. A biomass wood waste (spruce bark) was employed to fabricate a composite doped with Si and Mg and applied to adsorb an emerging contaminant (Omeprazole) from aqueous solutions, as well as synthetic effluents loaded with several emerging contaminants. The effects of Si and Mg doping on the biobased material's physicochemical properties and adsorptive performance were evaluated. Si and Mg did not influence the specific surface area values but impacted the presence of the higher number of mesopores. The kinetic and equilibrium data presented the best fitness by the Avrami Fractional order (AFO) and Liu isotherm models, respectively. The values of Q_{max} ranged from 72.70 to 110.2 mg g⁻¹ (BP) and from 107.6 to 249.0 mg g⁻¹ (BTM). The kinetic was faster for Si/Mg-doped carbon adsorbent, possibly due to different chemical features provoked by the doping process. The thermodynamic data showed that the adsorption of OME on biobased adsorbents was spontaneous and favorable at four studied temperatures (283, 293, 298, 303, 308, 313, and 318 K), with the magnitude of the adsorption correspondent to a physical adsorption process ($\Delta H^\circ < 2$ kJ mol⁻¹). The adsorbents were applied to treat synthetic hospital effluents and exhibited a high percentage of removal (up to 62%). The results of this work show that the composite between spruce bark biomass and Si/Mg was an efficient adsorbent for OME removal. Therefore, this study can help open new strategies for developing sustainable and effective adsorbents to tackle water pollution.

Keywords: wood waste; magnesium carbon dopant; silica carbon dopant; adsorption; omeprazole



Citation: Teixeira, R.A.; Thue, P.S.; Lima, É.C.; Grimm, A.; Naushad, M.; Dotto, G.L.; dos Reis, G.S.

Adsorption of Omeprazole on Biobased Adsorbents Doped with Si/Mg: Kinetic, Equilibrium, and Thermodynamic Studies. *Molecules* **2023**, *28*, 4591. <https://doi.org/10.3390/molecules28124591>

Academic Editor: Marcello Brigante

Received: 21 April 2023

Revised: 3 June 2023

Accepted: 5 June 2023

Published: 6 June 2023



Copyright: © 2023 by the authors. Licensee MDPI, Basel, Switzerland. This article is an open access article distributed under the terms and conditions of the Creative Commons Attribution (CC BY) license (<https://creativecommons.org/licenses/by/4.0/>).

1. Introduction

Nowadays, the pollution of water bodies is a tremendous issue for the environment, animals, and human beings, and due to the intense human and industrial activities, this issue has only grown [1,2]. Among many different pollutants in natural waters, a new class, so-called emerging contaminants (ECs), has gathered enormous concerns from environmental researchers due to their deleterious effects on living beings, even at very small concentrations [3,4]. ECs are different compounds, such as pharmaceuticals and

personal care products, plasticizers, food additives, wood preservatives, laundry detergents, surfactants, disinfectants, pesticides, hormones, etc. [3]. ECs are unregulated or not completely regulated compounds, even in the most developed countries; therefore, they must be properly removed from wastewater before being discharged into the environment. However, ECs cannot be easily removed from wastewater under traditional wastewater treatment techniques [3,4].

There are several methods employed to treat effluents loaded with ECs, including advanced oxidation procedures [5], biological treatment [6], photocatalysis [7], filtration [8], and adsorption [9–11]. However, most of these treatment methods are not techno-economically feasible for field implementation. Furthermore, these developed methods have some problems due to the complex procedures, maintenance, high investment cost, toxic byproduct generation, etc. In addition, they can generate toxic sludges, which need further costs for sludge management and disposal [5–7]. Therefore, a more suitable treatment process for removing ECs is required, and adsorption appears as one of the most suitable treatment methods due to its high-efficiency removal, low initial implementation and operational costs, easy operation, and controllable residue generation.

In order to achieve an effective adsorption process, selecting and designing a suitable and efficient adsorbent must be met [12–14]. Among the most popular adsorbents, activated carbon (AC) is widely popular and effectively employed [12–14]. Activated carbons are well-known for their excellent adsorption characteristics due to their highly developed pore structure, elevated surface area, and essential surface activity [12,13]. However, ACs possess the disadvantages of relatively complex synthesis processes—mainly during the activation step—that usually employ high amounts of chemicals such as zinc chloride and potassium hydroxide (usually a ratio of 1:1 of chemical/biomass) [15–18]. Moreover, a washing step with hydrochloric acid is needed to remove the remaining chemical activator after the pyrolysis process [19–22]. These steps are directly correlated with the high costs of activated carbon preparation.

Each biobased carbon adsorbent property deeply depends on the pyrolysis conditions and chemical/dopant used, as these impact its adsorptive performances due to enhancing its active surface sites [16,17]. For instance, doping the carbon matrix with Si and Mg increases adsorptive active sites [18]. This work prepared biobased adsorbent materials using biomass wood waste (spruce bark). As far as we know, for the first time, we report the preparation of new composite biobased materials doped with Si and Mg and subsequently used to adsorb an emerging contaminant (Omeprazole) from aqueous solutions. Furthermore, the effect of doping on the biochar's final physicochemical properties was subjected to a deep investigation. This paper successfully improves sustainable strategies for developing high-performance biomass-based adsorbents to remove EC from wastewater. This research is expected to help open new strategies for developing sustainable and effective adsorbents to tackle water pollution.

2. Results and Discussion

2.1. Characterization of the Adsorbents

Textural properties such as SSA and porosity (meso- and micropore features) are very important for determining any adsorbent's quality that will impact its adsorptive performances [22,23]. The textural characteristics of the biobased adsorbents (BP and BTM) are summarized in Table 1. It shows that the chemical dopants used did not influence the SSA value. Both samples exhibited SSA values of 205 and 202 $\text{m}^2 \text{g}^{-1}$ for BP and BTM, respectively. Compared with the literature, Deng et al. [24] prepared corncob biochars doped with MgCl_2 and obtained specific surface areas ranging from 52.41 to 174.29 $\text{m}^2 \text{g}^{-1}$. Although there was no difference in SSA values, the doping Si/Mg did influence the mesopore contribution compared to the pristine biobased carbon. The mesopores are responsible for adsorbing molecules larger in size, and also it could improve the uptake of smaller molecules since each pore of the material can accommodate agglomerates of small molecules [12,14]. However, the results show that both adsorbents are highly

microporous, which is a good characteristic that may facilitate the diffusion of smaller adsorbate molecules such as OME into the adsorbents' pores [25].

Table 1. Textural properties of BP and BTM.

Samples	SSA ($\text{m}^2 \text{g}^{-1}$)	A_{Mic} ($\text{m}^2 \text{g}^{-1}$)	A_{Mes} ($\text{m}^2 \text{g}^{-1}$)	Pore Vol. ($\text{cm}^3 \text{g}^{-1}$)
BP	205	191	14	0.24
BTM	202	168	33	0.22

The surface morphological characteristics of BP and B-Si-Mg adsorbents are evaluated by SEM images (shown in Figure 1). BP exhibits a more irregular surface with no apparent porosity. In contrast, BTM showed a smoother surface with several small holes unveiling some developed porous structures related to a high surface area. On the doped biochar's surface, it is possible to observe some white dots, which are the dopants attached (fused) to the biochar carbon matrix. It is reported that adsorbents rich in both physical (irregular morphology) and chemical (by introducing Si/Mg atoms) defects can be beneficial in adsorbing OME because these defects act as adsorptive sites that can boost the adsorption through pore filling and electrostatic interaction (further explained ahead in the mechanism of adsorption) [11,13,17]. Complementarily to SEM, EDS mapping of Si (Figure 1c) and Mg (Figure 1d) is also explored. EDS quantification of the elements indicated 18.4% and 10.7% of Si and Mg, respectively. The elements mapping of the composite surface confirmed the presence of two elements (Si and Mg), showing their uniform distribution over the carbon structure (see Figure 2c,d).

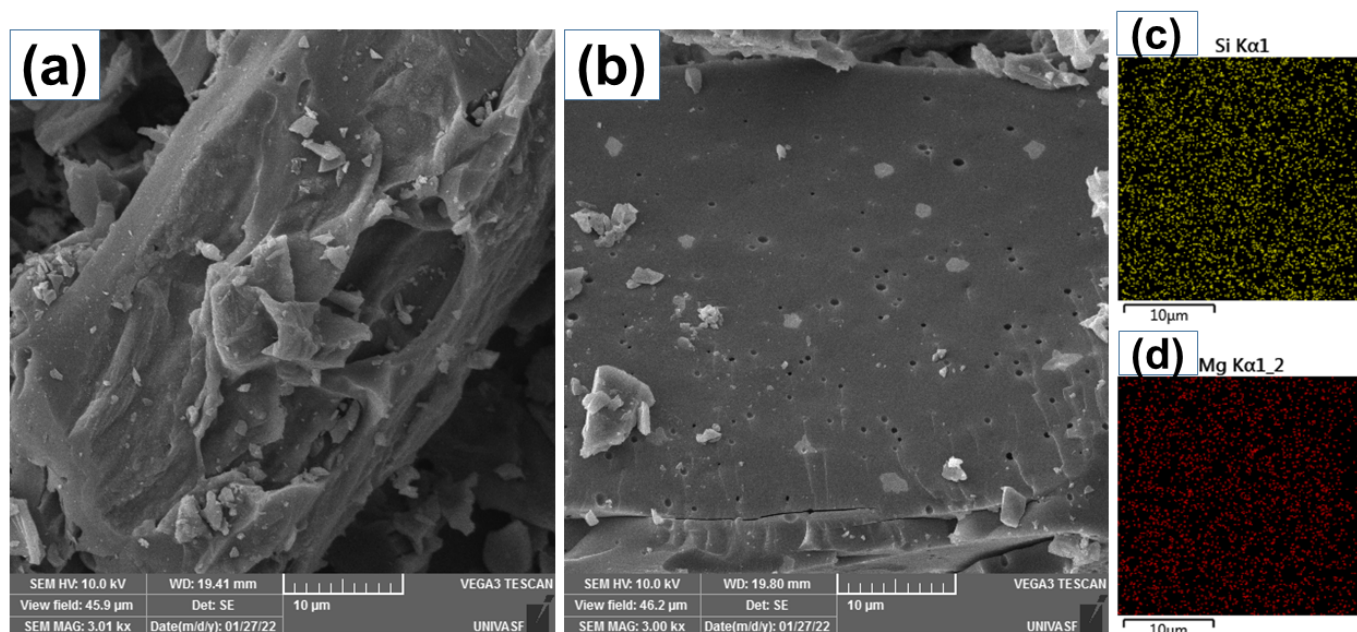


Figure 1. SEM images of (a) BP; (b) BTM; (c) Si mapping for BTM, and (d) Mg mapping for BTM.

Figure 2 shows the Raman analysis for both samples; Raman spectroscopy gives valuable information on the order/disorder and degrees of biochars graphitization [26,27]. Figure 2 shows that for both samples, two characteristic peaks at 1335 cm^{-1} (D-band) and 1600 cm^{-1} (G-band). The D-band is related to C atoms of defects or disordered structures, typically dominant in amorphous carbon materials derived from biomass, while G-band represents carbon atoms with an sp^2 electronic configuration in graphite structures [28–30]. In addition, from the Raman spectrum, the ratio between D and G peaks ($I_{\text{D}}/I_{\text{G}}$) is often employed to determine the degree of graphitization of the biochar.

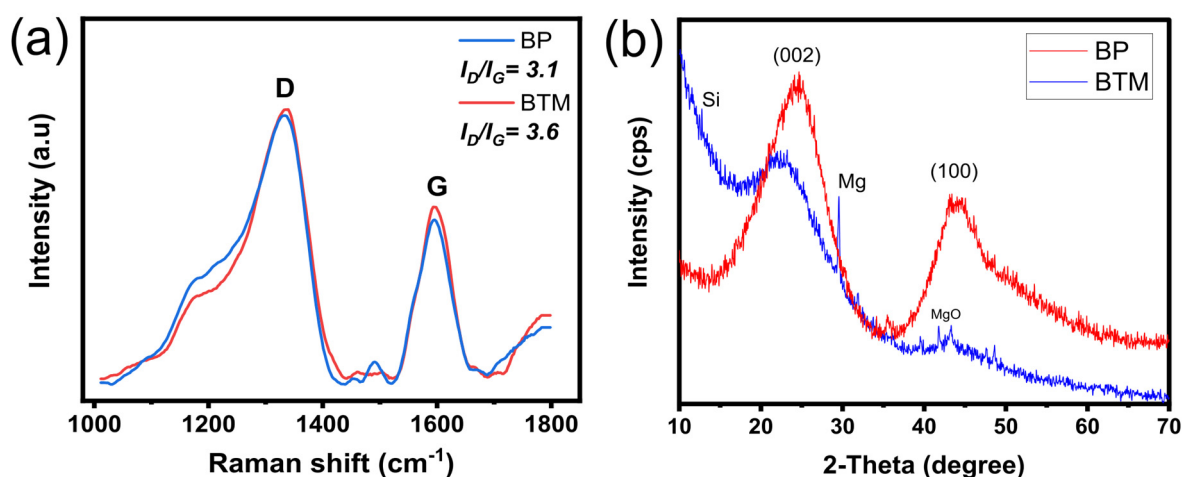


Figure 2. Raman spectra (a) and XRD patterns (b) of the adsorbent materials.

The carbon material doped with the Si/Mg presented a slightly higher I_D/I_G (3.6) compared to pure carbon sample BP (3.2) (see Figure 2a), indicating little more defects in its structure. Many reports suggest that adsorbents rich in defects, which could mean more adsorption sites, can have their adsorptive properties boosted [11]. As previously mentioned, these defects can be both physical and chemical, which are responsible for boosting the adsorbent adsorptive properties through different mechanisms (pore filling and electrostatic interactions, further explained ahead in Section 2.5). Therefore, Si/Mg dopants helped increase the adsorption sites in the BTM adsorbent.

Figure 2b shows the X-ray diffraction pattern of the adsorbent materials. Important differences are observed between both patterns (see Figure 2b). BP shows two prominent broad peaks at $2\theta = 24.5^\circ$ and 44° , which are associated with the (002) and (100) planes, respectively [31,32]. The (002) peak is attributed to the packed carbon layers and amorphous and aliphatic structures [31,32]. The broad peak at 44° is associated with (100) diffractions of graphitic carbons, indicating a certain degree of aromatization in the BP structure. However, for the BTM, the broad peak at (100) disappeared, indicating a higher degree of amorphization, possibly provoked by the incorporation of Si [32]. In addition, however, some small crystalline peaks can be seen related to MgO [24].

2.2. Kinetic of OME Adsorption on BP and BTM Adsorbents

In an adsorption process, the kinetic is a crucial step to ensure that the system reaches the saturated adsorption capacity and for understanding the mechanism(s) acting in the process regarding diffusion and mass transport in the adsorption system [29–33]. Figure 3 and Table 1 show the kinetic curves and parameters for OME removal onto biobased adsorbents, respectively. The same trend was observed for both adsorbents, with a rapid increase in their uptake within 25 min, which seemed to reach the equilibrium (see Figure 3). The rapid equilibrium highlights the high affinity between adsorbents and adsorbate.

The nonlinear pseudo-first-order (PFO), pseudo-second-order (PSO), and Avrami-fractional-order (AFO) models were used to analyze the fitness of the kinetic data (see Table 2 and Figure 3). It is essential to understand the adsorption rate to design the adsorbents' application. In this study, nonlinear models were used, which offer a good fitting of the data. PFO and PSO models suppose that the interaction between adsorbate and adsorbent can be physical or chemical adsorption, following an adsorption kinetic of first or second order, respectively. However, the AFO model suggests a fractional order of the adsorption kinetic. The models' fitness was evaluated using the adjusted R^2_{adj} , SD, and BIC values [14,25,34] (see Supplementary Materials).

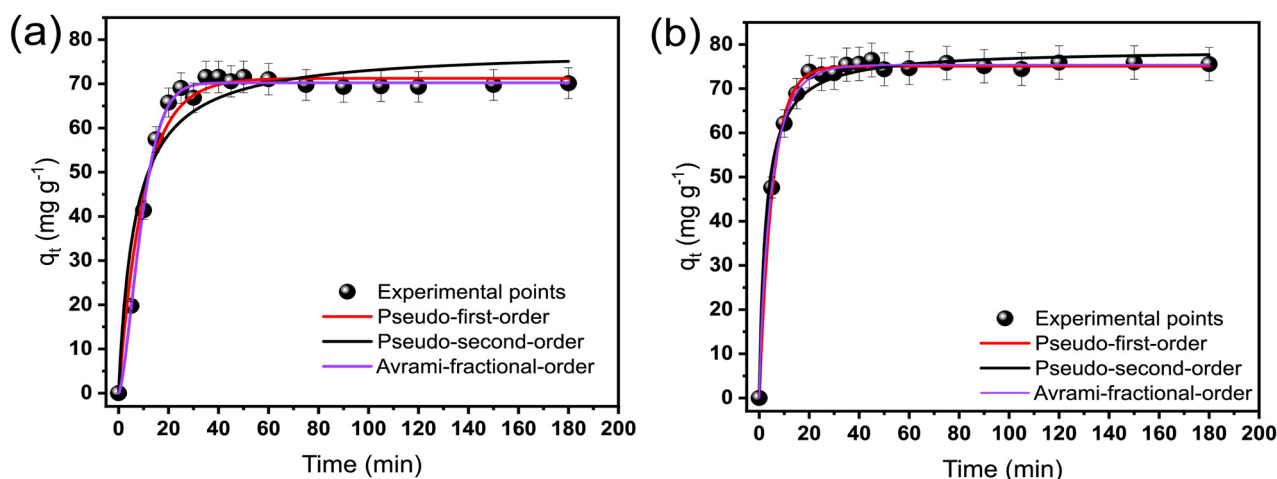


Figure 3. OME kinetic of adsorption curves on BP (a) and BTM (b) adsorbents. Conditions: adsorbate concentration of 300 mg L^{-1} , temperature of $25 \text{ }^\circ\text{C}$, adsorbent dosage of 1.5 g L^{-1} , and initial solution pH 7.0.

Table 2. OME kinetic adsorption parameters on BP and BTM adsorbents.

	BP	BTM
Pseudo-first order		
$q_e \text{ (mg g}^{-1}\text{)}$	71.25	75.09
$k_1 \text{ (min}^{-1}\text{)}$	0.09760	0.1874
$t_{1/2} \text{ (min)}$	7.105	3.699
$t_{0.95} \text{ (min)}$	30.71	15.99
$R^2 \text{ adjusted}$	0.9782	0.9967
$SD \text{ (mg g}^{-1}\text{)}$	8.861	1.121
BIC	45.82	8.610
Pseudo-second order		
$q_e \text{ (mg g}^{-1}\text{)}$	77.86	78.82
$k_2 \text{ (g mg}^{-1} \text{ min}^{-1}\text{)}$	1.941×10^{-3}	4.840×10^{-3}
$t_{1/2} \text{ (min)}$	6.613	2.622
$t_{0.95} \text{ (min)}$	125.7	49.83
$R^2 \text{ adjusted}$	0.9200	0.9869
$SD \text{ (mg g}^{-1}\text{)}$	32.55	4.440
BIC	69.24	33.37
Avrami fractional order		
$q_e \text{ (mg g}^{-1}\text{)}$	70.23	75.42
$k_{AV} \text{ (min}^{-1}\text{)}$	0.09433	0.1977
n_{AV}	1.515	0.8409
$t_{1/2} \text{ (min)}$	8.320	3.270
$t_{0.95} \text{ (min)}$	21.87	18.65
$R^2 \text{ adjusted}$	0.9969	0.9981
$SD \text{ (mg g}^{-1}\text{)}$	1.266	0.6329
BIC	12.53	0.04500

Lower SD and higher R^2_{adj} values suggest that the q experimental values are much closer to q provided by the models. Thus, it better describes the experimental values, suggesting the model's better fitness. As seen in Table 2, AFO exhibited the highest R^2_{adj} and lowest SD values and, therefore, better suitability to describe the kinetic adsorption of OME on both adsorbents. Moreover, the Bayesian Information Criterion (BIC) was also employed to corroborate the suitability of the kinetic model. Lima et al. (2021) [21] reported that if the difference between two BIC values (ΔBIC) of the models is ≤ 2.0 , it means that the difference between the two models is not significant. For $\Delta\text{BIC} \geq 10$, it can be stated

without any doubt that the model with a lower BIC value presented the best suitability. Table 2 shows that the Δ BIC values between the AFO model and PFO were 33.29 and 8.57, and the BIC differences between the AFO model and PSO were 56.71 and 33.33 for BP and BTM, respectively. This confirms that the AFO kinetic model for the OME molecules adsorption is the best-fitted. The adsorption order for the OME molecules on BP was 1.513, a value closer to 2, while n_{AV} for the adsorption of OME molecules onto BTM was 0.8409, a value close to 1.

The AFO is widely reported in the literature, and it suggests a complex process with multiple adsorption pathways, with dynamic/different mechanism (s), while adsorption occurs [35,36]. This process presents multiple kinetic orders instead of one, represented by n_{AV} , which usually has a fractional value [35,36]. Thus, evaluating $t_{1/2}$ and $t_{0.95}$ becomes important for comparing different kinetic models (see Table 2) [19,20,25,33–35]. The $t_{0.95}$ is the time to reach 95% of total saturation, and $t_{1/2}$ is the time to reach 50%. Considering that the AFO presented the best fitness, its values for $t_{1/2}$ and $t_{0.95}$ were 8.32 min and 21.87 min, and 3.27 min and 18.65 min for BP and BTM adsorbents. It shows that the kinetic was faster for BTM, possibly due to different chemical features provoked by the doping with Si/Mg [24]. Short times to attain 95% saturation are obtained for carbon-based materials to uptake emerging organic molecules [12,14,20].

2.3. Equilibrium Isotherms Studies of OME on Biobased Adsorbents

The isotherm of adsorption is a valuable tool for better evaluating the adsorption system between the adsorbent and adsorbate [37–41]. There are many isotherm models, and in this work, the Langmuir, Freundlich, and Liu models were employed to study the equilibrium of adsorption between adsorbents and OME molecules [37,42–44]. Freundlich's model assumes multiple layers of adsorbate covering the adsorbent. As a result, no saturation of the adsorbent is achieved, and the energy of each active site is not homogeneous, while Langmuir almost assumes the opposite. Liu is the combination of Freundlich and Langmuir models and considers the saturation of the adsorbent, a multilayer of the adsorption of adsorbate, and the activate sites of the adsorbents with different energy [39,40,44].

The isotherm curves and parameters are displayed in Figure 4 and Table 3. The fitness of the isotherm models was examined previously for the kinetics (by R^2_{adj} , SD, and BIC values). Considering the SD values and R^2_{adj} obtained from the nonlinear isotherm model fitting, high differences were observed between the models for all temperatures. In general, Liu's model provided the lowest SD and highest R^2_{adj} values for both adsorbents. Moreover, taking into account the BIC values, they were lowest for Liu, which is statistically the best-chosen model [14,20,34]. The Liu model assumes that the adsorbent's adsorption active sites cannot have the same energy. Therefore, the adsorbents may present active sites preferred by the OME molecules for occupation. However, at the studied condition, the saturation of the active sites should occur, unlike in the Freundlich isotherm model. Except for the isotherm at 298 K, Table 3 shows a fitting for the Liu isotherm model. This may indicate that the surface of the biobased adsorbents is likely heterogeneous, with different energy adsorption sites.

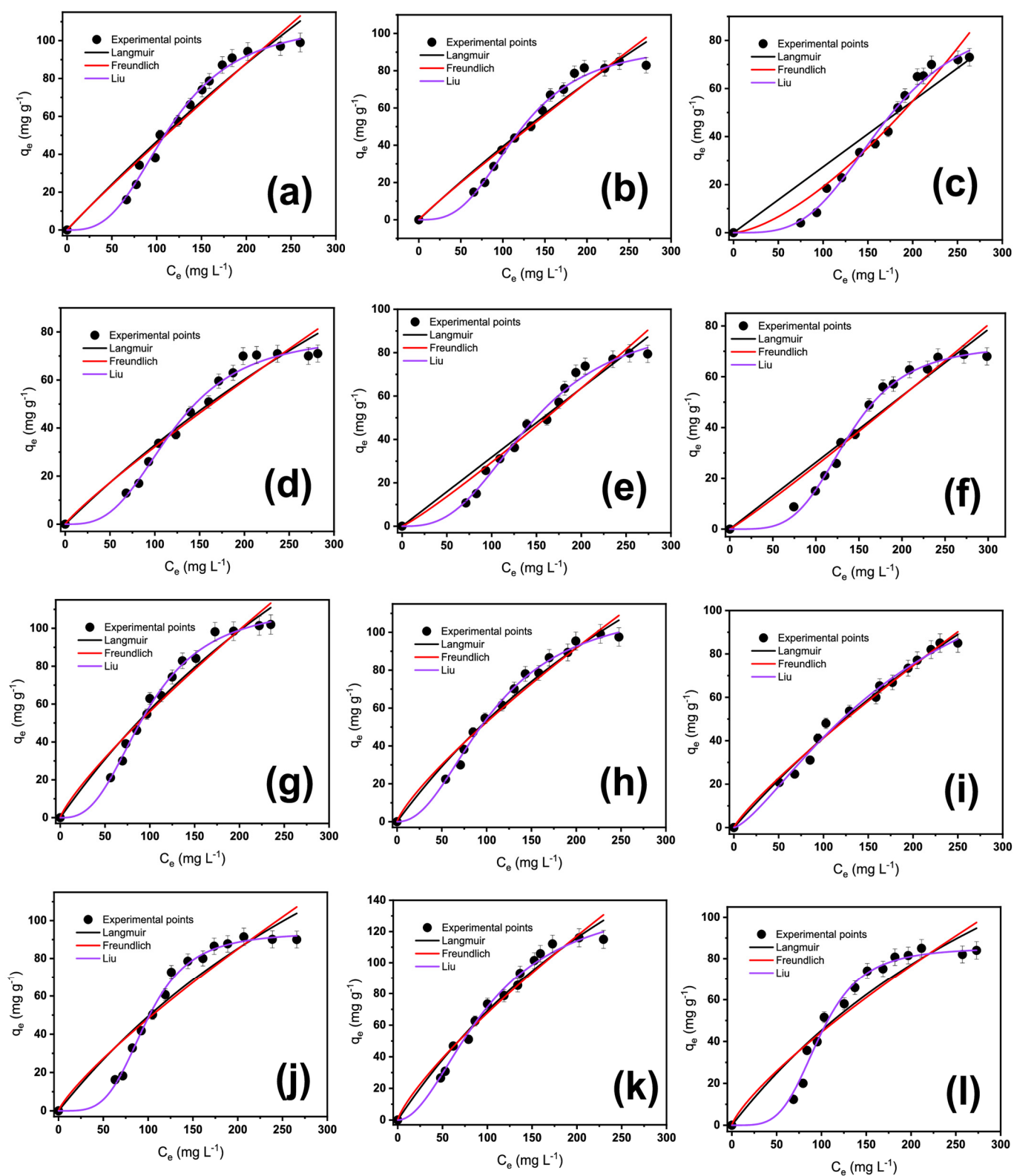


Figure 4. OME isotherms of adsorption curves at different temperatures for BP, (a) 283 K, (b) 293 K, (c) 298 K, (d) 303 K, (e) 313 K, and (f) 318 K; and for BTM (g) 283 K, (h) 293 K, (i) 298 K, (j) 303 K, (k) 313 K, and (l) 318 K. Conditions: Adsorbent dosage of 1.5 g L^{-1} , and initial pH solution 7.0.

Table 3. Langmuir, Freundlich, and Liu isotherm parameters for omeprazole (OME) adsorption on Norway Spruce Bark adsorbents BP and BTM.

BP						
Temperature in K	283	293	298	303	313	318
Langmuir						
Q_{\max} (mg g ⁻¹)	730.9	582.9	511.0	351.2	417	133
K_L (L mg ⁻¹)	68.31×10^{-5}	7.24×10^{-4}	5.36×10^{-8}	1.04×10^{-3}	7.63×10^{-7}	1.98×10^{-5}
R^2_{adj}	0.9288	0.9278	0.8723	0.9208	0.9369	0.8992
SD (mg g ⁻¹)	73.30	56.63	85.57	46.20	45.32	55.98
BIC	70.40	66.53	72.72	63.47	63.18	66.35
Freundlich						
K_F (mg g ⁻¹ (mg L ⁻¹) ^{-1/nF})	0.5770	0.4990	0.0170	0.5260	0.1780	0.1870
n_F	1.054	1.061	0.659	1.119	0.901	0.9410
R^2_{adj}	0.9234	0.9220	0.9458	0.9114	0.9427	0.9012
SD (mg g ⁻¹)	78.79	61.22	36.29	51.69	41.16	54.85
BIC	71.48	67.70	59.85	65.16	61.74	66.05
Liu						
Q_{\max} (mg g ⁻¹)	110.2	94.62	91.54	79.04	96.21	72.70
K_g (L mg ⁻¹)	0.008600	0.008400	0.005900	0.008300	0.006900	0.007270
n_L	2.951	2.974	3.508	3.041	2.795	4.080
R^2_{adj}	0.9906	0.9891	0.9855	0.9852	0.9857	0.9925
SD (mg g ⁻¹)	9.648	8.518	9.739	8.627	10.23	4.140
BIC	41.48	39.62	41.63	39.81	42.37	28.80
BTM						
Temperature in K	283	293	298	303	313	318
Langmuir						
Q_{\max} (mg g ⁻¹)	260.1	208.9	310.9	220.7	256.9	263.8
K_L (L mg ⁻¹)	3.59×10^{-3}	4.45×10^{-3}	1.92×10^{-3}	4.37×10^{-3}	4.54×10^{-3}	3.23×10^{-3}
R^2_{adj}	0.9839	0.9426	0.9909	0.9567	0.9784	0.9602
SD (mg g ⁻¹)	17.74	59.45	7.251	46.00	29.10	43.19
BIC	49.12	67.25	35.70	63.41	56.54	62.46
Freundlich						
K_F (mg g ⁻¹ (mg L ⁻¹) ^{-1/nF})	2.603	3.207	1.314	3.1309	3.4704	2.2674
n_F	1.416	1.549	1.267	1.515	1.479	1.384
R^2_{adj}	0.9721	0.9149	0.9922	0.9326	0.9649	0.9427
SD (mg g ⁻¹)	30.73	88.14	6.181	71.59	47.26	62.17
BIC	57.36	73.16	33.30	70.04	63.81	67.93
Liu						
Q_{\max} (mg g ⁻¹)	146.9	107.6	249.0	112.2	152.9	118.2
K_g (L mg ⁻¹)	0.009500	0.01260	1.109×10^{-8}	0.01280	0.01120	0.01140
n_L	1.564	2.565	0.7892	2.404	1.566	2.276
R^2_{adj}	0.9915	0.9906	0.9916	0.9955	0.9855	0.9918
SD (mg g ⁻¹)	9.336	9.692	6.696	4.817	19.46	8.864
BIC	40.99	41.55	36.01	31.07	52.01	40.21

2.4. Thermodynamic Studies of OME on BP and BTM

The thermodynamics was examined using the van't Hoff approach [22], whose equilibrium constant was accessed from the best equilibrium constant obtained in the isotherms from 283 to 318 K. Table 4 shows the thermodynamic adsorption parameters for OME on biobased adsorbents. The thermodynamic data show that the adsorption process was spontaneous and favorable at the six studied temperatures (283, 293, 298, 303, 308, 313, and 318 K), with negative values of ΔG° [20,33,34,45]. Furthermore, the adsorption process was endothermic for BTM adsorbent ($\Delta H^\circ < 0$) and exothermic for BP ($\Delta H^\circ > 0$) [20,33,45]. The ΔH° values refer to the magnitude of the adsorption [20,33,35,45], which corresponds to a physical adsorption process since its values are < 40 kJ mol⁻¹ [35,45]; however, other mechanisms could be involved in the adsorption of OME on BP and BTM, which is further studied in the next section. Finally, for both adsorbents, the changes in the entropy (ΔS°)

were positive, which indicates an increase in the randomness, and a more disorganized state of the adsorption system, after OME uptake by BP and BTM [31,32,46].

Table 4. Thermodynamic parameters of OME adsorption on BP and BTM adsorbents.

Temperature (K)	283	293	298	303	313	318
Liu model						
BP						
K_e^0	2980.8	2897.9	2055.1	2853.004	2379.8	2763.2
ΔG° (kJ mol ⁻¹)	-18.82	-19.42	-18.89	-20.04	-20.23	-20.95
ΔH° (kJ mol ⁻¹)	-	-	-1.581	-	-	-
ΔS° (J K ⁻¹ mol ⁻¹)	-	-	60.90	-	-	-
R^2	-	-	0.9930	-	-	-
R^2_{adj}	-	-	0.9895	-	-	-
BTM						
K_e^0	3274.4	4348.6	663.2	4403.9	3865.0	3947.9
ΔG° (kJ mol ⁻¹)	-19.04	-20.41	-16.10	-21.14	-21.49	-21.89
ΔH° (kJ mol ⁻¹)	-	-	4.022	-	-	-
ΔS° (J K ⁻¹ mol ⁻¹)	-	-	81.50	-	-	-
R^2	-	-	0.9997	-	-	-
R^2_{adj}	-	-	0.9995	-	-	-

2.5. Mechanism of Adsorption

An adsorption mechanism between OME and BTM can be stated based on the biochars' physicochemical characteristics (porosity and chemical surface and functionalities) and adsorption results. The high adsorption of OME by the BTM adsorbent was achieved due to its physical features through the pore-filling mechanism and chemical interactions through H-bonding, π - π and n- π interactions, and the Lewis acid–base interaction [9–12,14] (see Figure 5). Since the biochars are very porous, physical adsorption through pore filling should be the principal mechanism involved in the process, although other mechanisms also take place in removing OME from the aqueous solution. In addition, the Mg on the carbon matrix generates dipoles in the carbon structure due to electronegativity differences that generate ion–dipole interaction with the OME molecules [18].

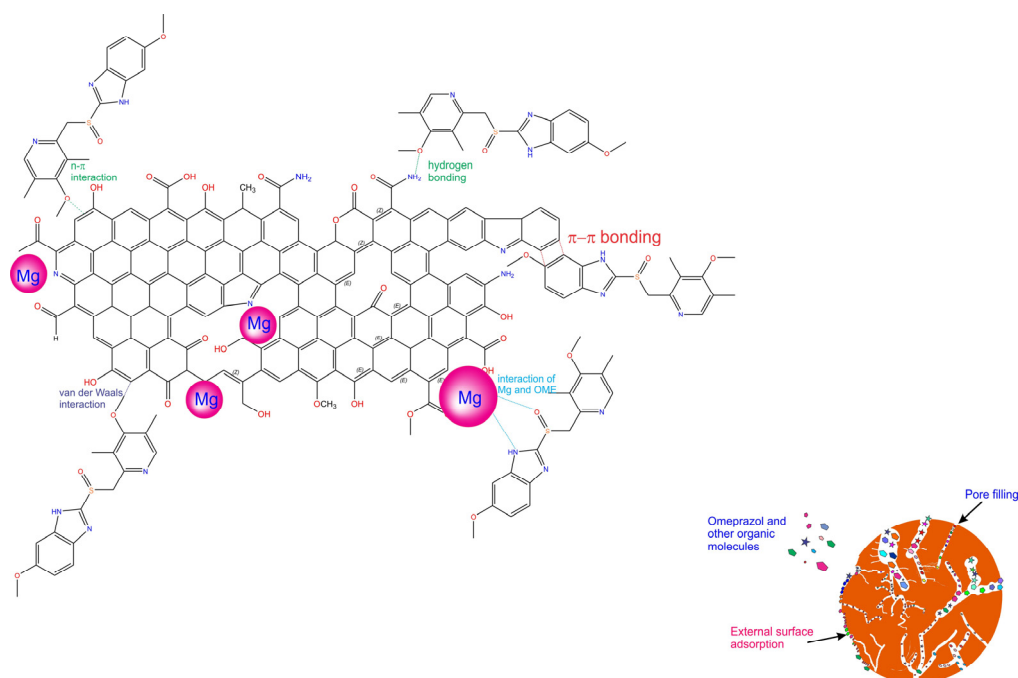


Figure 5. Mechanism of adsorption of OME onto BTM adsorbent.

2.6. Synthetic Effluent Treatment Tests

The biobased adsorbents showed good efficiency in removing OME from aqueous solutions. Thus, they are expected to be effective in treating effluents containing several organic and inorganic compounds (similar to real effluents). Therefore, two synthetic wastewaters loaded with several drugs, and other organic and inorganic compounds (see Supplementary Table S1) were employed to test the ability of the BP and BTM to clean them up (see Figure 6).

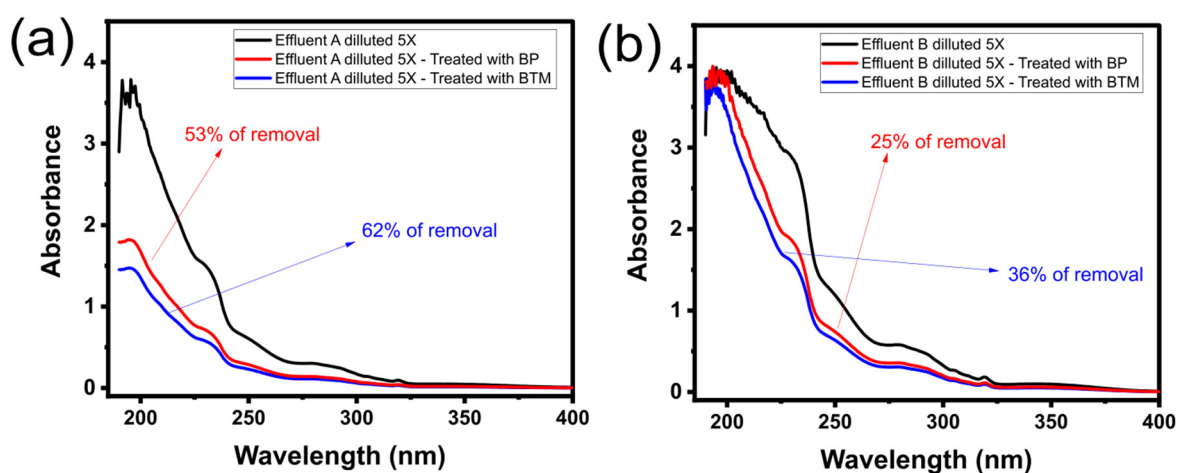


Figure 6. Spectra of effluents A (a) and B (b) treated by BP and BTM adsorbents.

The percentage of removal of the effluents' compounds was measured while taking into account the UV–Vis spectra area of the two synthetic effluents before and after the treatment under the band of absorption from 190 to 500 nm [10,11,19,47] (see Figure 6). The results showed that BTM adsorbent removed 62% and 36% of the total compounds from the synthetic effluents A (lowly concentrated) and B (highly concentrated), respectively, while BP adsorbent removed 53% and 25% for effluents A and B, respectively. The better BTM efficiency in removing both effluents matches the previous adsorption results that exhibited better performances for the BTM adsorbent. These results suggest that the adsorbents prepared in this work could be employed in real effluents carried with drugs and other organic/inorganic pollutants.

3. Materials and Methods

3.1. Preparation of the Adsorbents-Activated Biochars

Spruce bark waste was used to produce the adsorbents. Firstly, the biomass waste was ground, using a hammer mill, to a particle size smaller than 0.5 mm. Then, for the doped sample (with Si and Mg), 10 g of biomass was mixed with 2 g of TEOS (tetraethyl orthosilicate) and 1 g of $MgCl_2$ into a solution of water/ethanol (50%:50%), under vigorous stirring at room temperature for 2 h. The function of adding TEOS to $MgCl_2$ is the possibility of forming Si-O-Mg bonds that could affect the sorption capacity of the BRM material. After that, the mixture was placed in a drying oven overnight at 80 °C. The same procedure was used for the pristine biobased material sample but without TEOS and $MgCl_2$. Next, the impregnated samples were pyrolyzed using a specially designed reactor at a temperature of 800 °C in a CO_2 flow for 1 h. After that, the temperature of the sample was increased to 10 °C/min. Finally, samples were ground using a hammer mill and sieved to a particle size < 200 μm . To wash away the remaining byproducts from the pyrolyzed carbon materials, they were washed several times with boiling de-ionized water until the pH of the wash water was equal to the pH of the de-ionized water. Hereafter, these samples were named BP (non-doped with Si/Mg) and BTM for the doped sample.

3.2. Characterization of the Biochars

The specific surface area (SSA) and micro/meso-pore structure were obtained using a sorption meter (Tristar 3000, Micromeritics Instrument Corp., Norcross, GA, USA). The samples were subjected to degasification at 180 °C for 3 h in a nitrogen atmosphere. The SSA was calculated using the Brunauer–Emmett–Teller (BET) method.

The adsorbents' surface morphology was examined by scanning electron microscopy (SEM) (55-VP, Supra, Zeiss, Jena, Germany), using an acceleration voltage of 20 kV. In addition, the Raman spectra of the adsorbents were obtained using a Bruker Bravo spectrometer (Bruker, Ettlingen, Germany).

The amorphous and crystalline nature of adsorbents were evaluated through X-ray diffraction, using an X-ray diffractometer (Bruker D8 Advance, Ettlingen, Germany), operating at 45 kV and 40 mA, using Cu-K α monochromatic radiation ($\lambda = 1.54 \text{ \AA}$), 2θ angle interval of 10–70 and a scan rate of 0.4°/min.

3.3. Adsorption Studies

De-ionized water was used to prepare the OME (omeprazole) solutions and the synthetic effluents. The batch mode was employed to evaluate the applicability of the biobased adsorbents in removing OME from aqueous solutions. In addition, the effect of the solution temperature on OME adsorption was investigated. All adsorption experiments were performed using 30 mg of each biochar into 20 mL of OME, using 50.0 mL Falcon tubes [18–20]. OME initial solution concentrations from 80 to 420 mg L⁻¹ were employed in the experiments for isotherms studies. The kinetic OME removal on biochars was studied, varying contact time from 0 to 180 min, with an OME initial concentration of 300 mg L⁻¹. The effect of temperature was measured, and thermodynamic studies were performed, at temperatures from 283 to 318 K. All adsorption experiments were performed at a constant shaking speed of 200 rpm. After adsorption, the residual solutions of OME were quantified using a UV-Visible spectrophotometer (Shimadzu 1800) at a maximum wavelength of 298 nm. The removal capacity and the percentage of OME removal are obtained from Supplementary Equations (S1) and (S2), respectively.

3.4. Kinetics, Equilibrium, and Thermodynamics Studies

The kinetics were studied by employing PFO, PSO, and AFO models. Three isotherm models, i.e., the Freundlich, Langmuir, and Liu models, were employed for the equilibrium study. The thermodynamics was examined from van't Hoff approach [21], whose equilibrium constant was accessed from the best equilibrium constant obtained in the isotherms from 283 to 318 K. Information on these models and their fitness suitability are shown in the Supplementary Materials.

3.5. Synthetic Effluents

Two simulated pharmaceutical effluents, which consisted of drugs and other organic/inorganics compounds found in hospital wastewater, were prepared with de-ionized water [9–11]. The compositions and concentrations of the components of the effluents are presented in Supplementary Table S1. The purpose of using simulated effluents is to test the sorption capacities of the adsorbents for the removal of the mixture of several compounds simulating real effluents.

4. Conclusions

In this work, we developed adsorbents with improved emerging contaminant (OME) adsorption skills. TEOS and MgCl₂ made carbon-based composite adsorbents as Si and Mg sources. The physicochemical characterization proved that successfully incorporating Si and Mg modified the carbon structure, yielding better adsorptive properties. The addition of Si and Mg in the carbon structure helped to increase the number of mesopores. The EDS quantification of the elements indicated 18.4% and 10.7% of Si and Mg, respectively. When tested as adsorbents, the AFO model better fitted the kinetic, and the equilibrium

data were better fitted to the Liu isotherm model. The adsorbent sample doped with both chemicals (Si and Mg) presented a faster kinetic, reaching 95% of their saturations at 21.87 and 18.65 min for BP and BTM adsorbents, respectively. The maximum adsorption capacities obtained from the Liu model at 298 K were 91.54 and 249.0 mg g⁻¹ for BP and BTM, respectively. The better adsorptive properties of the BTM were due to different chemical features provoked by the doping process. The thermodynamic data showed that the adsorption of OME on biobased adsorbents was spontaneous and favorable at the range of studied temperatures, with the magnitude of the adsorption corresponding to the physical adsorption process. The adsorbents were applied in treating synthetic hospital effluents containing different pharmaceuticals, organics, and inorganic salts and presented a high percentage of removal (up to 62%). The results of this work have shown that the composite between spruce bark biomass and Si/Mg was an efficient adsorbent for emerging pollutants removal. Therefore, we hope this report can help open new strategies for developing sustainable and effective adsorbents to tackle water pollution.

Supplementary Materials: The following are available online at <https://www.mdpi.com/article/10.3390/molecules28124591/s1>, “Information about Adsorption on Kinetic, Equilibrium, and Thermodynamic Models and Calculations”; Table S1: Chemical composition of simulated synthetic effluents.

Author Contributions: Conceptualization, G.S.d.R. and P.S.T.; methodology, G.S.d.R., R.A.T. and P.S.T.; validation, É.C.L.; formal analysis, G.S.d.R., R.A.T. and P.S.T.; investigation, G.S.d.R., R.A.T. and P.S.T.; data curation, É.C.L. and A.G.; writing—original draft, G.S.d.R.; writing—review and editing, É.C.L., M.N., A.G. and G.L.D.; funding acquisition, É.C.L. and M.N. All authors have read and agreed to the published version of the manuscript.

Funding: The authors are grateful to the Researchers Supporting Project number (RSP2023R8), King Saud University, Riyadh, Saudi Arabia, for the financial support. The authors are also grateful to Bio4Energy and SLU (Sweden), CAPES, and CNPq (Brazil) for financing part of this current research.

Institutional Review Board Statement: Not applicable.

Informed Consent Statement: Not applicable.

Data Availability Statement: Not applicable.

Acknowledgments: Dos Reis thanks Bio4Energy—a Strategic Research Environment appointed by the Swedish government and the Swedish University of Agricultural Sciences (SLU)—for the funding support. Alejandro Grimm acknowledges financial support from the Swedish Research Council FORMAS (2021-00877). The authors are grateful to the Researchers Supporting Project number (RSP2023R8), King Saud University, Riyadh, Saudi Arabia, for the financial support. CAPES and CNPq from Brazil also financed part of this current research.

Conflicts of Interest: The authors declare no conflict of interest.

References

1. Evgenidou, E.N.; Konstantinou, I.K.; Lambropoulou, D.A. Occurrence and removal of transformation products of PPCPs and illicit drugs in wastewaters: A review. *Sci. Total Environ.* **2015**, *505*, 905–926. [[CrossRef](#)] [[PubMed](#)]
2. Imwene, K.O.; Ngumba, E.; Kairigo, P.K. Emerging technologies for enhanced removal of residual antibiotics from source-separated urine and wastewaters: A review. *J. Environ. Manag.* **2022**, *322*, 116065. [[CrossRef](#)] [[PubMed](#)]
3. Carmalin, S.A.; Lima, E. Removal of emerging contaminants from the environment by adsorption. *Ecotoxicol. Environ. Saf.* **2018**, *150*, 1–17.
4. Li, X.; Wang, B.; Liu, F.; Yu, G. Occurrence and Removal of Pharmaceutical Contaminants in Urine: A Review. *Water* **2023**, *15*, 1517. [[CrossRef](#)]
5. Ibanez, M.; Gracia-Lor, E.; Bijlsma, L.; Morales, E.; Pastor, L.; Hernández, F. Removal of emerging contaminants in sewage water subjected to advanced oxidation with ozone. *J. Hazard. Mater.* **2013**, *260*, 389–398. [[CrossRef](#)] [[PubMed](#)]
6. de Oliveira, J.F.; Fia, R.; Rodrigues, F.N.; Fia, F.R.L.; de Matos, M.P.; Siniscalchi, L.A.B.; Sanson, A.L. Quantification, removal and potential ecological risk of emerging contaminants in different organic loads of swine wastewater treated by integrated biological reactors. *Chemosphere* **2020**, *260*, 127516. [[CrossRef](#)]
7. Isac, L.; Cazan, C.; Andronic, L.; Enesca, A. CuS-Based Nanostructures as Catalysts for Organic Pollutants Photodegradation. *Catalysts* **2022**, *12*, 1135. [[CrossRef](#)]

8. Ferreira, V.; Gómez-Motos, I.; Lombrana, J.I.; de Luis, A.; Villota, N.; Ros, O.; Etxebarria, N. Contaminants of emerging concern removal in the effluent of wastewater treatment plant under biological and continuous mode ultrafiltration treatment. *Water* **2020**, *12*, 725. [[CrossRef](#)]
9. Thue, P.S.; Umpierrez, C.S.; Lima, E.C.; Lima, D.R.; Machado, F.M.; dos Reis, G.S.; da Silva, R.S.; Pavan, F.A.; Tran, H.N. Single-step pyrolysis for producing magnetic activated carbon from tucumã (*Astrocaryum aculeatum*) seed and nickel(II) chloride and zinc(II) chloride. Application for removal of Nicotinamide and Propanolol. *J. Hazard Mater.* **2020**, *398*, 122903. [[CrossRef](#)]
10. dos Reis, G.S.; Guy, M.; Mathieu, M.; Jebrane, M.; Lima, E.C.; Thyrel, M.; Dotto, G.L.; Larsson, S.H. A Comparative Study of Chemical Treatment by MgCl₂, ZnSO₄, ZnCl₂, and KOH on Physicochemical Properties and Acetaminophen Adsorption Performance of Biobased Porous Materials from Tree Bark Residues. *Colloids Surf. A Physicochem. Eng. Asp.* **2022**, *642*, 128626. [[CrossRef](#)]
11. González-Hourcade, M.; Simões dos Reis, G.; Grimm, A.; Dinh, V.M.; Lima, E.C.; Larsson, S.H.; Gentili, F.G. Microalgae Biomass as a Sustainable Precursor to Produce Nitrogen-Doped Biochar for Efficient Removal of Emerging Pollutants from Aqueous Media. *J. Clean. Prod.* **2022**, *348*, 131280. [[CrossRef](#)]
12. Lima, E.C.; Naushad, M.; dos Reis, G.S.; Dotto, G.L.; Pavan, F.A.; Guleria, A.; Seliem, M.K.; Sher, F. Production of carbon-based adsorbents from lignocellulosic biomass. In *Biomass-Derived Materials for Environmental Applications*; Anastopoulos, I., Lima, E.C., Meili, L., Giannakoudakis, D.A., Eds.; Elsevier: Amsterdam, The Netherlands, 2022; pp. 169–191, ISBN 978-0-323-91914-2.
13. Ahmad, T.; Manzar, M.S.; Georgin, J.; Franco, D.S.P.; Khan, S.; Meili, L.; Ullah, N. Development of a new hyper crosslinked resin based on polyamine-isocyanurate for the efficient removal of endocrine disruptor bisphenol-A from water. *J. Water Proc. Eng.* **2023**, *53*, 103623. [[CrossRef](#)]
14. Cimirro, N.F.G.M.; Lima, E.C.; Cunha, M.R.; Grimm, P.S.T.A.; dos Reis, G.S.; Rabiee, N.; Saeb, M.R.; Keivanimehr, F.; Habibzadeh, S. Removal of diphenols using pine biochar. Kinetics, equilibrium, thermodynamics, and mechanism of uptake. *J. Mol. Liq.* **2022**, *364*, 119979. [[CrossRef](#)]
15. Lima, D.R.; Lima, E.C.; Thue, P.S.; Dias, S.L.P.; Machado, F.M.; Seliem, M.K.; Sher, F.; dos Reis, G.S.; Saeb, M.R.; Rinklebe, J. Comparison of acidic leaching using a conventional and ultrasound-assisted method for preparation of magnetic-activated biochar. *J. Environ. Chem. Eng.* **2021**, *9*, 105865. [[CrossRef](#)]
16. dos Reis, G.S.; Larsson, S.H.; Mathieu, M.; Thyrel, M.; Pham, T.N. Application of design of experiments (DoE) for optimised production of micro- and mesoporous Norway spruce bark activated carbons. *Biomass Convers. Biorefinery* **2021**, 1–19. [[CrossRef](#)]
17. dos Reis, G.S.; Bergna, D.; Tuomikoski, S.; Grimm, A.; Lima, E.C.; Thyrel, M.; Skoglund, N.; Lassi, U.; Larsson, S.H. Preparation and characterization of pulp and paper mill sludge-activated biochars using alkaline activation: A box–Behnken design approach. *ACS Omega* **2022**, *7*, 32620–32630. [[CrossRef](#)]
18. Lee, Y.-E.; Jeong, Y.; Shin, D.-C.; Ahn, K.-H.; Jung, J.-H.; Kim, I.-T. Fabrication of Mg-Doped Sargassum Biochar for Phosphate and Ammonium Recovery. *Sustainability* **2021**, *13*, 12752. [[CrossRef](#)]
19. Cai, L.; Zhang, Y.; Ma, R.; Feng, X.; Yan, L.; Jia, D.; Xu, M.; Ai, L.; Guo, N.; Wang, L. Nitrogen-Doped Hierarchical Porous Carbon Derived from Coal for High-Performance Supercapacitor. *Molecules* **2023**, *28*, 3660. [[CrossRef](#)]
20. dos Reis, G.S.; Larsson, S.H.; Thyrel, M.; Pham, T.N.; Claudio Lima, E.; de Oliveira, H.P.; Dotto, G.L. Preparation and Application of Efficient Biobased Carbon Adsorbents Prepared from Spruce Bark Residues for Efficient Removal of Reactive Dyes and Colors from Synthetic Effluents. *Coatings* **2021**, *11*, 772. [[CrossRef](#)]
21. Cunha, M.R.; Lima, E.C.; Lima, D.R.; da Silva, R.S.; Thue, P.S.; Seliem, M.K.; Sher, F.; dos Reis, G.S.; Larsson, S.H. Removal of captoril pharmaceutical from synthetic pharmaceutical-industry wastewaters: Use of activated carbon derived from *Butia catarinensis*. *J. Environ. Chem. Eng.* **2020**, *8*, 104506. [[CrossRef](#)]
22. Lima, E.C.; Hosseini-Bandegharaei, A.; Moreno-Piraján, J.C.; Anastopoulos, I. A critical review of the estimation of the thermodynamic parameters on adsorption equilibria. Wrong use of equilibrium constant in the Van't Hoof equation for calculation of thermodynamic parameters of adsorption. *J. Mol. Liq.* **2019**, *273*, 425–434. [[CrossRef](#)]
23. Efevbokhan, V.E.; Alagbe, E.; Odika, B.; Babalola, R.; Oladimeji, T.E.; Abatan, O.G.; Yusuf, E.O. Preparation and characterization of activated carbon from plantain peel and coconut shell using biological activators. *J. Phys. Conf. Ser.* **2019**, *1378*, 032035. [[CrossRef](#)]
24. Thommes, M.; Kaneko, K.; Neimark, A.V.; Olivier, J.P.; Rodriguez-Reinoso, F.; Rouquerol, J. Physisorption of gases, with special reference to the evaluation of the surface area and pore size distribution (IUPAC technical report). *Pure Appl. Chem.* **2015**, *87*, 1051–1069. [[CrossRef](#)]
25. Deng, Y.; Li, X.; Ni, F.; Liu, Q.; Yang, Y.; Wang, M.; Ao, T.; Chen, W. Synthesis of Magnesium Modified Biochar for Removing Copper, Lead, and Cadmium in Single and Binary Systems from Aqueous Solutions: Adsorption Mechanism. *Water* **2021**, *13*, 599. [[CrossRef](#)]
26. Guy, M.; Mathieu, M.; Anastopoulos, I.P.; Martínez, M.G.; Rousseau, F.; Dotto, G.L.; de Oliveira, H.P.; Lima, E.C.; Thyrel, M.; Larsson, S.H.; et al. Process Parameters Optimization, Characterization, and Application of KOH-Activated Norway Spruce Bark Graphitic Biochars for Efficient Azo Dye Adsorption. *Molecules* **2022**, *27*, 456. [[CrossRef](#)]
27. Larkin, P. *Infrared and Raman Spectroscopy: Principles and Spectral Interpretation*; Elsevier: Amsterdam, The Netherlands, 2011.
28. Smith, E.; Dent, G. *Modern Raman Spectroscopy—A Practical Approach*; John Wiley and Sons: Hoboken, NJ, USA, 2005; pp. 1–210.
29. Song, X.; Ma, X.; Li, Y.; Ding, L.; Jiang, R. Tea waste-derived microporous active carbon with enhanced double-layer supercapacitor behaviors. *Appl. Surf. Sci.* **2019**, *487*, 189–197. [[CrossRef](#)]

30. Huang, G.G.; Liu, Y.F.; Wu, X.-X.; Cai, J.-J. Activated carbons prepared by the KOH activation of a hydrochar from garlic peel and their CO₂ adsorption performance. *New Carbon Mater.* **2019**, *34*, 247–257. [[CrossRef](#)]
31. Sun, L.; Tian, C.; Li, M.; Meng, X.; Wang, L.; Wang, R.; Yin, J.; Fu, H. From coconut shell to porous graphene-like nanosheets for high-power supercapacitors. *J. Mater. Chem. A* **2013**, *1*, 6462–6470. [[CrossRef](#)]
32. Mansuri, I.; Farzana, R.; Rajarao, R.; Sahajwalla, V. Carbon Dissolution Using Waste Biomass—A Sustainable Approach for Iron-Carbon Alloy Production. *Metals* **2018**, *8*, 290. [[CrossRef](#)]
33. Han, Y.; Lin, N.; Xu, T.; Li, T.; Tian, J.; Zhu, Y.; Qian, Y. An amorphous Si material with a sponge-like structure as an anode for Li-ion and Na-ion batteries. *Nanoscale* **2018**, *10*, 3153. [[CrossRef](#)]
34. Cavalcante, E.H.M.; Candido, I.C.M.; de Oliveira, H.P.; Silveira, K.B.; Alvares, T.V.S.; Lima, E.C.; Thyrel, M.; Larsson, S.H.; dos Reis, G.S. 3-Aminopropyl-triethoxysilane functionalized tannin-rich grape biomass for the adsorption of methyl orange dye: Synthesis, characterization, and the adsorption mechanism. *ACS Omega* **2022**, *7*, 18997–19009. [[CrossRef](#)] [[PubMed](#)]
35. dos Reis, G.S.; Pinto, D.; Lima, E.C.; Knani, S.; Grimm, A.; Silva, L.F.O.; Cadaval Jr, T.R.S.; Dotto, G. Lanthanum uptake from water using chitosan with different configurations. *React. Funct. Polym.* **2022**, *180*, 105395. [[CrossRef](#)]
36. Grimm, A.; dos Reis, G.S.; Dinh, V.M.; Larsson, S.H.; Mikkola, J.P.; Lima, E.C.; Xiong, S.J. Hardwood spent mushroom substrate-based activated biochar as a sustainable bioresource for removal of emerging pollutants from wastewater. *Biomass. Convers. Biorefinery* **2022**. [[CrossRef](#)]
37. Oladoja, N.A. A critical review of the applicability of Avrami fractional kinetic equation in adsorption-based water treatment studies. *Desalin. Water Treat.* **2015**, *57*, 15813–15825. [[CrossRef](#)]
38. Choi, A.E.S.; Roces, S.A.; Dugos, N.P.; Wan, M.W. Adsorption of sulfones from actual oxidized diesel oil in the frame of oxidative desulfurization: A process optimization study using activated clay. *J. Clean. Prod.* **2022**, *363*, 132357. [[CrossRef](#)]
39. Choi, A.E.S.; Roces, S.A.; Dugos, N.P.; Wan, M.W. Adsorption of benzothiophene sulfone over clay mineral adsorbents in the frame of oxidative desulfurization. *Fuel* **2017**, *205*, 153–160. [[CrossRef](#)]
40. Choi, A.E.S.; Roces, S.A.; Dugos, N.P.; Arcega, A.; Wan, M.W. Adsorptive removal of dibenzothiophene sulfone from fuel oil using clay material adsorbents. *J. Clean. Prod.* **2017**, *161*, 267–276. [[CrossRef](#)]
41. Wang, J.; Guo, X. Adsorption isotherm models: Classification, physical meaning, application and solving method. *Chemosphere* **2020**, *258*, 127279. [[CrossRef](#)]
42. Ahmed, W.; Mehmood, S.; Qaswar, M.; Ali, S.; Khan, Z.H.; Ying, H.; Chen, D.Y.; Núñez-Delgado, A. Oxidized biochar obtained from rice straw as adsorbent to remove uranium (VI) from aqueous solutions. *J. Environ. Chem. Eng.* **2021**, *9*, 105104. [[CrossRef](#)]
43. Ranguin, R.; Ncibi, M.C.; Cesaire, T.; Lavoie, S.; Jean-Marius, C.; Grutzmacher, H.; Gaspard, S. Development and characterization of nanostructured hybrid material with vitamin B12 and bagasse-derived activated carbon for anaerobic chlordecone (Kepone) removal. *Environ. Sci. Pollut. Res. Int.* **2020**, *27*, 41122–41131. [[CrossRef](#)]
44. Chandra, I.K.; Ju, Y.-H.; Ayucitra, A.; Ismadji, S. Evans blue removal from wastewater by rarasaponin-bentonite. *Int. J. Environ. Sci. Technol.* **2013**, *10*, 359–370. [[CrossRef](#)]
45. Kefif, F.; Ezziane, K.; Bahmani, A.; Bettahar, N.; Mayouf, S. Evans Blue dye removal from contaminated water on calcined and uncalcined box [Cu-Al-CO]₃ Cu-Al-CO₃ layered double hydroxide materials prepared by coprecipitation. *Bull. Mater. Sci.* **2019**, *42*, 14. [[CrossRef](#)]
46. Lima, V.V.C.; Dalla Nora, F.B.; Peres, E.C.; Reis, G.S.; Lima, E.C.; Oliveira, M.L.S.; Dotto, G.L. Synthesis and characterization of biopolymers functionalized with APTES (3-aminopropyltriethoxysilane) for the adsorption of sunset yellow dye. *J. Environ. Chem. Eng.* **2019**, *7*, 103410. [[CrossRef](#)]
47. Reis, G.S.; Bergna, D.; Grimm, A.; Lima, E.C.; Hu, T.; Naushad, M.; Lassi, U. Preparation of highly porous nitrogen-doped biochar derived from birch tree wastes with superior dye removal performance. *Colloids Surf. A Physicochem. Eng. Asp.* **2023**, *669*, 131493. [[CrossRef](#)]

Disclaimer/Publisher's Note: The statements, opinions and data contained in all publications are solely those of the individual author(s) and contributor(s) and not of MDPI and/or the editor(s). MDPI and/or the editor(s) disclaim responsibility for any injury to people or property resulting from any ideas, methods, instructions or products referred to in the content.